Cobalt Homeostatic Catalysis for Coupling of Enaminones and Oxadiazolones to Quinazolinones

Weiping Wu,[§] Shuaixin Fan,[§] Xuan Wu, Lili Fang, and Jin Zhu*

Department of Polymer Science and Engineering, School of Chemistry and Chemical Engineering, State Key Laboratory of Coordination Chemistry, Nanjing University, Nanjing 210023, China.

[§]These authors contributed equally to this work.

*Corresponding Author (email: jinz@nju.edu.cn).

Abstract: Transition metal catalysis has revolutionized modern synthetic chemistry for its diverse modes of coordination reactivity. However, this versatility in reactivity is also the predominant cause of catalyst deactivation, a persisting issue that can significantly compromise its synthetic value. Homeostatic catalysis, a catalytic process that can sustain its productive catalytic cycle even when chemically disturbed, is proposed herein as an effective tactic to address the challenge. In particular, a cobalt homeostatic catalysis process has been developed for water-tolerant coupling of enaminones and oxadiazolones to quinazolinones. Dynamic covalent bonding serves as a mechanistic handle for preferred buffering of water onto enaminone and reverse exchange back by released secondary amine, thus securing reversible entry into cobalt dormant and active states for productive catalysis. Through this homeostatic catalysis mode, a broad structural scope has been achieved for quinazolinones, enabling further elaboration into distinct pharmaceutically active agents.

Keywords: Homeostatic Catalysis; Cobalt; Enaminone; Oxadiazolone; Quinazolinone.

Introduction

Transition metal catalysis has revolutionized the practice of modern synthetic chemistry, with significant impact in both academia and industrial settings.[1-4] A hallmark of this important class of chemical processes is the diverse modes of reactivity enabled by metal-ligand interactions.[5] This translates to the ability to synthesize a broad range of structurally distinct chemicals through the execution of on-target catalytic cycles. However, this supposedly appealing feature of reactivity diversity can also, inadvertently, result in the exit of originally catalytically active species to an undesired off-target reaction course and lead to off-loop catalyst dormancy or deactivation. Indeed, off-loop catalyst dormancy and deactivation are two frequently encountered issues in catalysis and can cause a tremendous loss of catalytic efficiency in catalytic process development if not properly addressed.[6,7] Herein we report the development of a homeostatic catalysis approach to combat these off-loop challenges. Homeostasis is a Nature's way of self-regulation that allows a biological system to maintain functional activity even in a hostile external environment.[8,9] One mechanism to achieve such a highly effective performance is through the localization of a dynamic and reversible chemical equilibrium process on a dedicated response unit so that no unintended, irreversible damage is inflicted upon the whole system. The homeostatic catalysis concept described herein recapitulates these mechanistic features and refers to a catalytic process that can sustain its productive catalytic cycle even when chemically disturbed. In particular, cobalt homeostatic catalysis permits the water-tolerant coupling of enaminones and oxadiazolones to quinazolinones. The adventitious inclusion of water into a catalytic system is practically unavoidable, given its ubiquitous presence in solvents, and has proven to be a major cause of catalyst deactivation in many different scenarios (Scheme 1a). For example, in heterogeneous catalysis, water can directly adsorb to the catalyst surface and block the active site[10,11] or induce activity-abolishing catalyst oxidation and sintering (Fischer-Tropsch catalyst);[12] in homogeneous catalysis,

hydrolytic ligand degradation and hydrolytic coordinate bond breakage (Ziegler-Natta catalyst, first- and second-generation Grubbs catalysts) can both elicit the loss of catalytic activity.[13-15] In our catalytic system (Scheme 1b), the highly labile C_{α}-N bond of enaminone (bearing a secondary amino group, either alone or when coordinated to cobalt) serves as the preferred buffering reactive site for water through dynamic covalent bonding-based nucleophilic exchange. This water-receptive reaction affords, initially, an off-loop, dormant cobalt enolate chelate of β-keto aldehyde and releases a secondary amine. However, the dynamic covalent bonding nature of the substitution enables the reversion of the reaction and the exchange back of hydroxyl group by the secondary amine, thus allowing its efficient on-loop re-entry back into the productive catalytic cycle. The expedient, precision dynamic covalent bonding exchange process provides a homeostatic catalysis mechanistic basis for preventing water from reacting elsewhere and exerting a deleterious, or even deactivating effect on the catalytic cycle.

Scheme 1. Effect of water on catalysts. (a) Deactivation of heterogeneous and homogeneous catalysts by water as reported previously. (b) Homeostatic catalysis concept proposed herein, as illustrated by dynamic covalent bonding-enabled receptive buffering of water and reverse exchange back in cobalt-catalyzed transformation of enaminones, eliminating the otherwise deleterious effect of water.

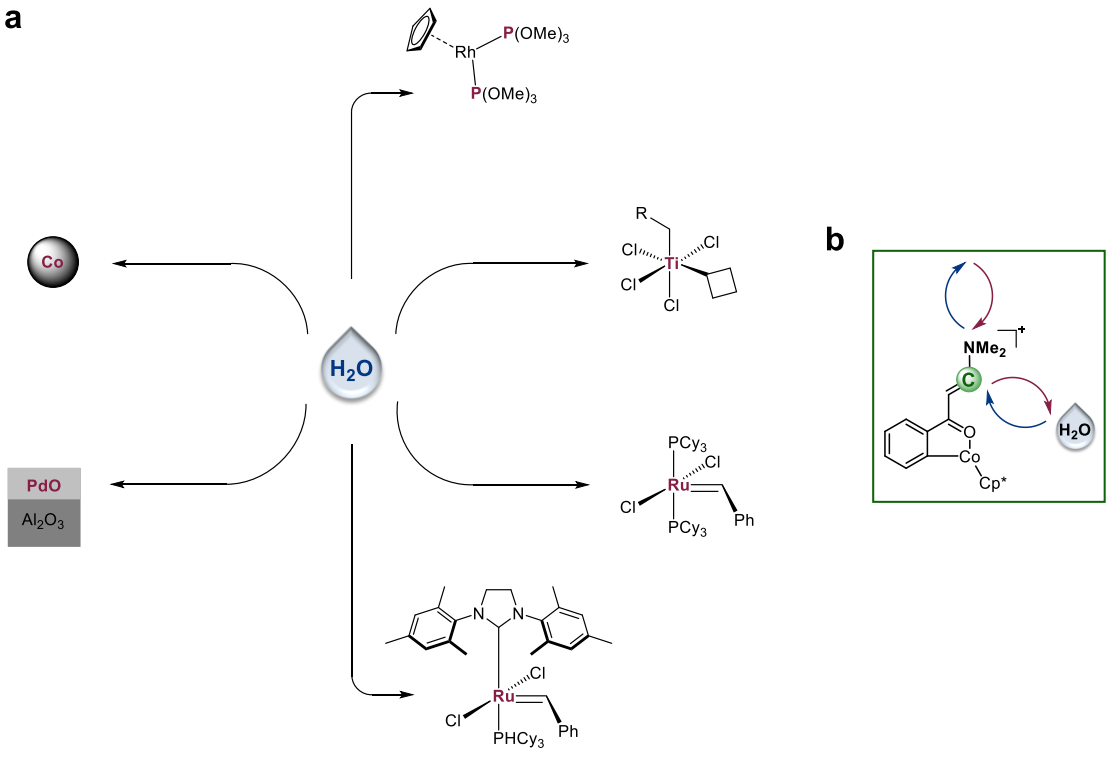

Enaminones are an important class of synthetic building blocks with intriguing both ambident eletrophilicity of enones (C_α and carbonyl C) and ambident nucleophilicity of enamines (N and C_β).[16,17] These versatile synthons have been used for transition-metal-catalyzed, directed C-H bond functionalization and cyclization reactions.[18,19] The cyclization reactions reported thus far are restricted to C-C bond formation at the C_β (dominant site, through its nucleophilicity) and C_α (minor site, through C-H bond activation).[20,21] Herein an intriguing mode of C-N bond formation at the carbonyl C site has been identified in coupling with oxadiazolones,[22] accompanied by a unique C_β-carbonyl C bond cleavage. The quinazolinone skeleton generated hereof has proven their privileged pharmacore role in an extensive spectrum of disease settings.[23] They have been harnessed as anti-bacterial, anti-fungal, anti-HIV, anti-malaria, anti-diabetes (ghrelin receptor antagonist), anticonvulsant, anti-inflammatory, anti-cancer (tyrosine kinase inhibitor), and analgesic agents.[24-32] Although a variety of methods have been invented for the construction of this molecular scaffold, requirement of multiple steps for functional group installation, reliance on rare metal catalysts, and restriction in substrate scope enormously limited their synthetic utility (Scheme 2).[33-36] The combination of a base metal cobalt catalyst with conveniently accessible and bench-stable enaminones and oxadiazolones will revamp the synthetic logic of the field.

Scheme 2. Synthetic strategies for the construction of quinazolinone skeleton.

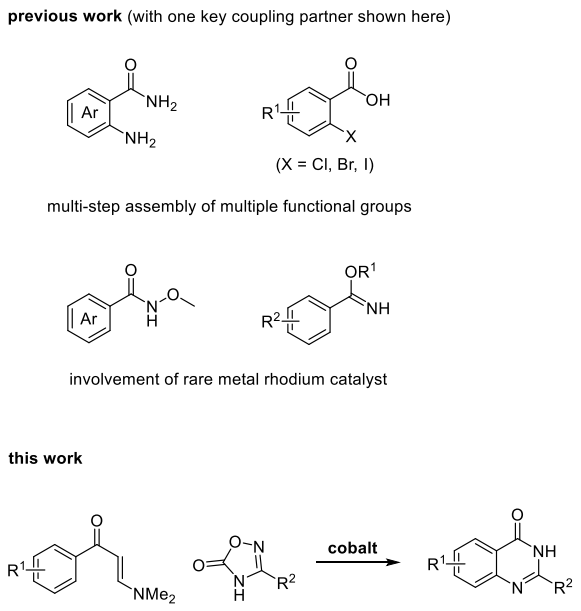

Results and Discussion

The investigation starts with the coupling reaction between (*E*)-3-dimethylamino-1-phenylprop-2-en-1-one (**1a**) and 3-phenyl-1,2,4-oxadiazol-5(4*H*)-one (**2a**) employing [CoCp*(CO)I_2] (10 mol %) as the catalyst precursor. Initial addition of 20 mol % (0.2 equiv) of $AgSbF_6$ in 2,2,2-trifluoroethanol (TFE) as a hypothetical iodide abstraction reagent gives a 20% yield of 2-phenylquinazolin-4(3*H*)-one (**3aa**, with structure unambiguously confirmed by single-crystal X-ray crystallography) at 110 °C under acidic condition (1.0 equiv HOAc). Alteration to a hypothetical ligand exchange reagent AgOAc (0.2 equiv) slightly lowers the yield to 16%. An increase of the total quantity of $AgSbF_6$ or AgOAc to 0.4 equiv raises the yield to over 30% level ($AgSbF_6$, 38%; AgOAc, 31%; $AgSbF_6$/AgOAc, 32%). Switch to a basic condition is detrimental to the reaction (LiOAc/$AgSbF_6$, 27%; CsOAc/$AgSbF_6$, 14%). With this basic screening results, the assessment of reaction conditions is then centered on the HOAc/$AgSbF_6$ combination. An elevation of the HOAc quantity to 2.0 equiv is not beneficial (34%). Instead, the yield is boosted to 49% when $AgSbF_6$ is varied to 1.0 equiv. A further change of the $AgSbF_6$ quantity to 2.0 equiv diminishes the yield to 38%. An alternative optimization on the HOAc side shows a surge of the yield to 54% and 62% (optimum) at a quantity of 0.5 and 0.2 equiv, respectively. A control experiment demonstrates the indispensability of HOAc for the transformation ($AgSbF_6$ alone, 19%). Deviation of the temperature from 110 °C exerts a negative impact on the reaction outcome (80 °C, 15%; 100 °C, 54%; 120 °C, 55%).

With the optimized reaction conditions (abbreviated hereafter as Co, Ag, H, TFE, 110 °C, 20 h) acquired, the substrate scope is next surveyed (Table 1). The enaminone scope is first evaluated by reacting with **2a**. For the *para* substitution on the phenyl ring of **1a**, both electron-donating and electron-withdrawing groups are compatible. Enaminones bearing both alkyl and cycloalkyl substituents display an essentially identical reactivity as the parent **1a** (**1b**, Me, 60%; **1c**, Et, 62%; **1d**,

^{i}Pr, 61%; **1e**, cyclohexyl, 63%). The fluoro substituent (**1f**) suppresses the reactivity to a 40% yield. The *ortho* substitution also allows the reaction to progress to a certain extent (**1g**, F, 35%). For the *meta* substitution, a single regioisomer, with cyclization occurring at the less sterically hindered site, is identified. A reduction in the reactivity is observed as compared to the *para* substitution (**1h**, Me, 56%; **1j**, F, 38%). The electron-donating methoxy substituent (**1i**, 42%) also provides a competent substrate. The *meta*, *para* disubstitution (**1k**, *m*-Me-*p*-Me, 54%) manifests the reactivity-attenuating effect of *meta* substitution.

Table 1. Substrate scope of enaminones.[a][b]

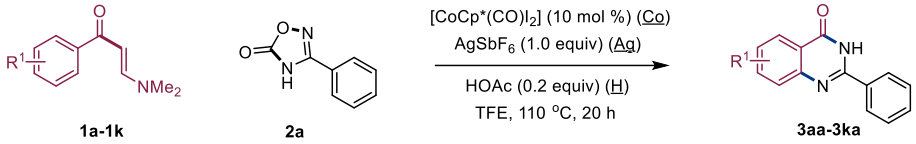

1a-1k **2a** **3aa-3ka**

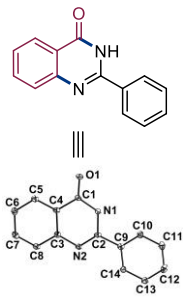

CCDC 2123836

3aa: R^1 = H, 62%

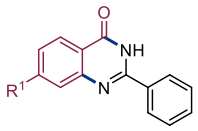

3ba: R^1 = Me, 60%
3ca: R^1 = Et, 62%
3da: R^1 = ^{i}Pr, 61%
3ea: R^1 = cyclohexyl, 63%
3fa: R^1 = F, 40%

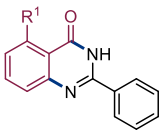

3ga: R^1 = F, 35%

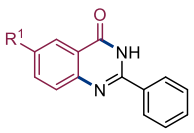

3ha: R^1 = Me, 56%
3ia: R^1 = OMe, 42%
3ja: R^1 = F, 38%

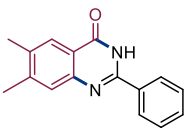

3ka: 54%

[a]Reaction conditions: **1a-1k** (0.24 mmol, 1.2 equiv), **2a** (0.2 mmol, 1.0 equiv), TFE (2.0 mL), under nitrogen. [b]Isolated yields.

The oxadiazolone scope is then examined by coupling with **1a** (Table 2). The reaction can proceed effectively across a broad span of structurally disparate substitution patterns. For the *para* substitution of **2a**, both electron-rich (**2b**, Me, 55%; **2c**, ^{i}Pr, 55%; **2d**, 4-ethylcyclohexyl, 55%; **2e**, OMe, 52%) and electron-poor (**2f**, F, 40%) substrates are capable of reacting smoothly, with electron-rich ones being higher-yielding. For the *ortho* substitution, the reactivity also shows group-dependent behavior, albeit in a different manner: methyl group (**2g**, 45%) imparts a lesser reactivity than the methoxy group (**2h**, 59%); the halide series witnesses a spike in reactivity for the bromo group (**2i**, F, 48%; **2j**, Cl, 48%; **2k**, Br, 60%; **2l**, I, 52%). For the *meta* substitution, the methyl analog (**2m**, 51%) is

inferior to the ethyl analog (**2n**, 57%) in product yield but indistinguishable from the methoxy counterpart (**2o**, 51%). The fluoro group (**2p**, 38%), similar to the case in the *para* substitution, retards the reaction. Disubstitution (**2q**, *m*-Me-*p*-Me, 51%; **2r**, *m*-OMe-*m*-OMe, 43%; **2s**, *m*-Me-*o*-F, 49%; **2t**, *p*-Me-*o*-Cl, 52%) poses no hurdle for the transformation and can even promote the reaction in certain circumstance (**2u**, *o*-Cl-*o*-Cl, 73%). With the complete replacement of phenyl group with a bulky 1-naphthyl group (**2v**, 32%), the yield falls almost to the half level. Significantly, diversification to the non-aromatic alkyl and alkenyl moieties retains the reactivity. The plain alkyl chain (**2w**, Me, 72%; **2x**, pentyl, 64%) affords a high-yielding substrate and additional linkage to an aromatic ring at the chain end is disadvantageous (**2y**, 4-methylbenzyl, 40%; **2z**, 2-phenylethyl, 44%). The yield also varies for the alkenyl substitution depending on the exact structure (**2a'**, 1-cyclohexenyl, 60%; **2b'**, styryl, 37%).

Table 2. Substrate scope of oxadiazolones.[a][b]

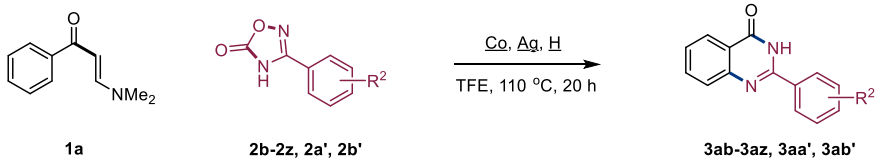

1a **2b-2z, 2a', 2b'** **3ab-3az, 3aa', 3ab'**

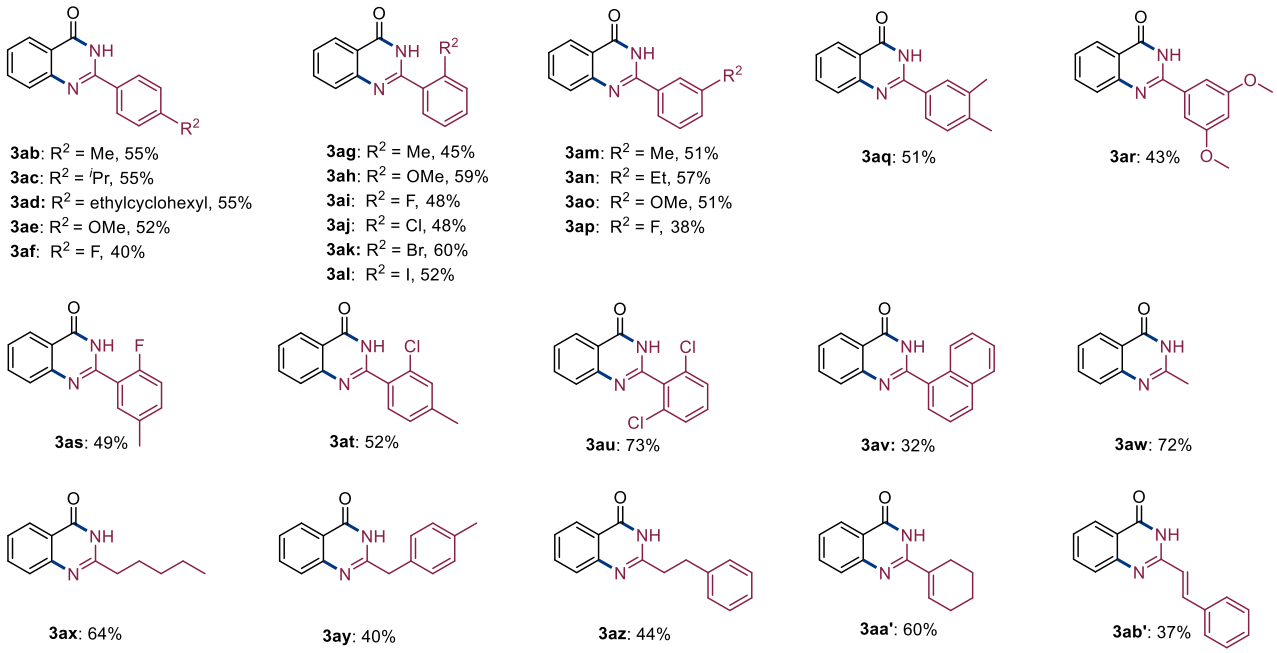

[a]Reaction conditions: **1a** (0.24 mmol, 1.2 equiv), **2a-2z, 2a', 2b'** (0.2 mmol, 1.0 equiv), TFE (2.0 mL), under nitrogen. [b]Isolated yields.

With the substrate scope inspected, a comprehensive series of experiments are performed to understand the reaction mechanism. An initial hint at the unusual nature of the catalytic process comes from an attempt at the isolation of catalytic intermediate (Scheme 3). A cobalt complex can indeed be isolated in catalysis involving **1a** and **2a**, albeit in small quantity (12% yield, calculated in reference to **2a**), under the modified condition of 0.7 equiv [CoCp*(CO)I_2] and 60 °C reaction temperature. The structure of the complex is unambiguously determined to be a deprotonated (*Z*)-3-hydroxy-1-phenylprop-2-en-1-one (**1a-OH**) chelate (**1a-O-Co-I**) of cobalt by single-crystal X-ray crystallography on an identical green complex prepared in large quantity by reacting **1a** with [CoCp*(CO)I_2] under either acidic or basic condition. Alternatively, **1a-O-Co-I** can be synthesized by direct deprotonated coordination of **1a-OH** with [CoCp*(CO)I_2]. It should be noted that while **1a-OH** is extremely unstable and prone to decomposition at room temperature (rt) or on column, **1a-O-Co-I** can readily undergo column chromatography purification. The evaluation of the reactivity of this apparently water-nucleophilic-substitution-derived cobalt complex toward **2a**, under catalysis-relevant condition, reveals no detectable product. Interestingly, an extra addition of $HNPh_2$ (in replacement of $HNMe_2$ because of the volatility issue), the hypothetical originally substitution-released by-product, revives the reaction to a 65% **3aa** yield. These results are consistent with the dynamic covalent bonding-enabled both formation of [**1a-O-Co**]$^+$ as the off-loop dormant species and its re-entry back into the catalytic cycle.

Scheme 3. Isolation of a dormant cobalt species and demonstration of its ability to re-gain reactivity.

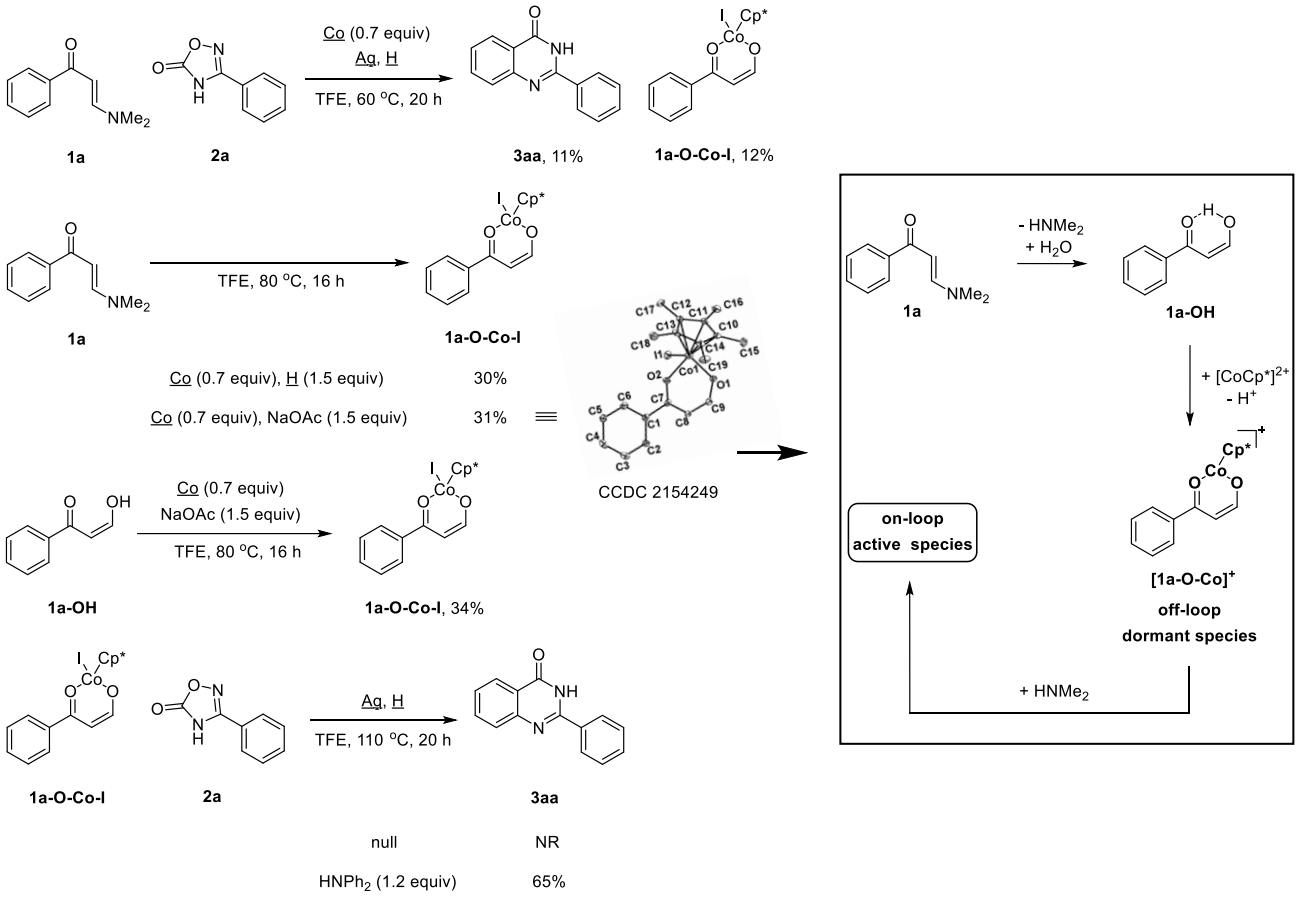

The existence of a dynamic covalent bonding exchange process is further validated by the following set of experiments (Scheme 4): forward hydrolytic generation of the by-product $HNPh_2$ (as a surrogate for the quantification of **1a-OH** yield), without the involvement of cobalt, from (*E*)-3-diphenylamino-1-phenylprop-2-en-1-one (**1a-NPh$_2$**, used instead of **1a** because of the purification issue arising from the instability of **1a-OH** and volatility of $HNMe_2$), reverse substitution reaction of either **1a-OH** (at rt or during the course of heating to 110 °C) or **1a-O-Co-I** (at 110 °C) with $HNPh_2$ to afford **1a-NPh$_2$**.

Scheme 4. Stoichiometric reactions showing the existence of a dynamic covalent bonding exchange process.

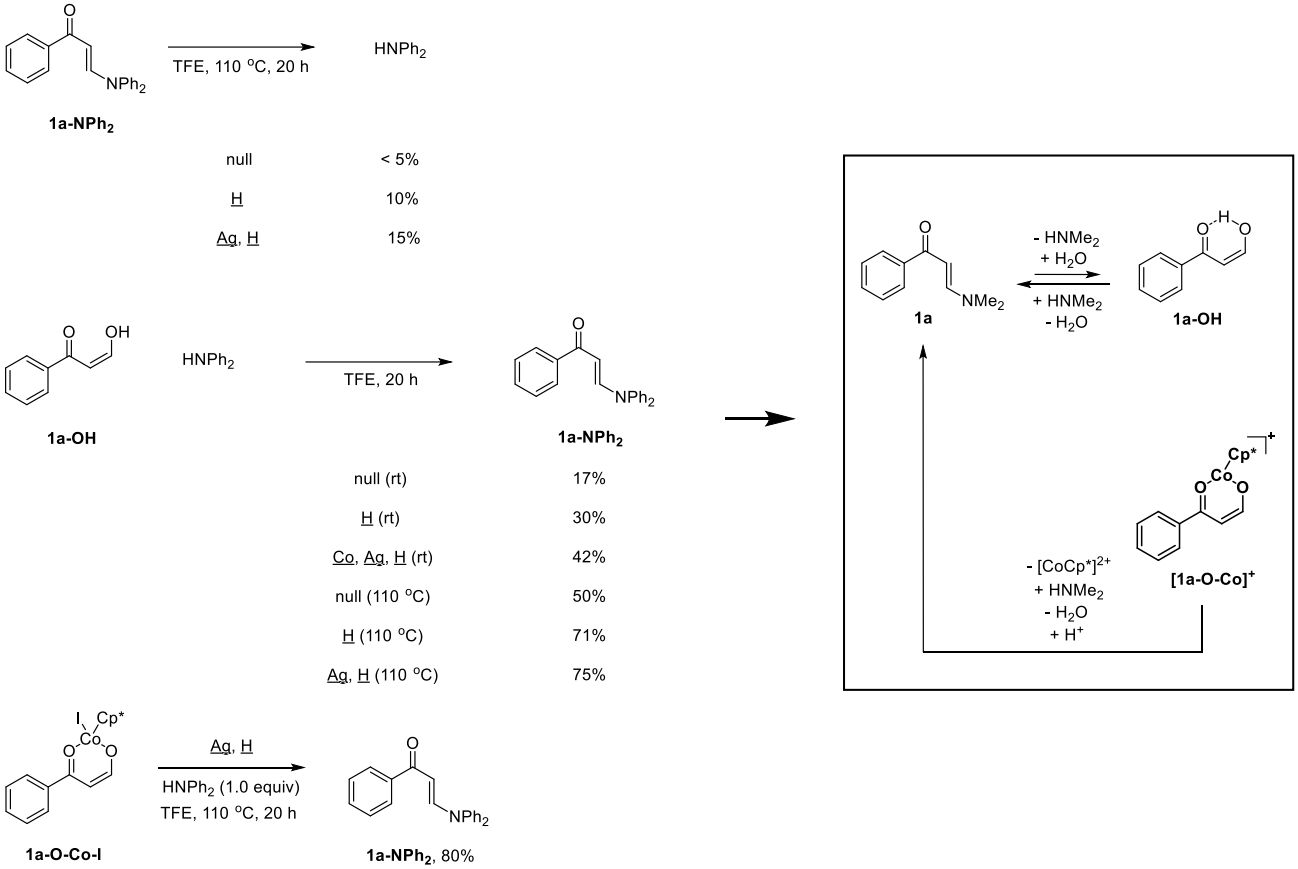

The structure of the catalytically active species from the reverse reaction of [**1a-O-Co**]$^{+}$ with $HNMe_2$ is speculated to be C-H bond-activated complex [**1a**$^{-H}$**-Co**]$^{+}$, as supported by the following lines of evidence (Scheme 5): the ability of **1a** fully deuterated at the phenyl ring (**1a-D$_5$**) to undergo D/H exchange (**1a-D$_5$-D/H**), the reactive production of D/H-exchanged **1a-D$_5$-O-Co-I-D/H** and **1a-D$_5$-D/H** under basic condition. The reverse reaction of **1a-OH** at 110 °C with $HNMe_2$ can not proceed directly because of the instability of **1a-OH** at this temperature, as manifested by the requirement of cobalt for mediating the forward-reverse exchange reaction between **1a** and $HNPh_2$. This exchange reaction carried out in the **1a-D$_5$** form witnesses a significant extent of D/H exchange, as informed by **1a-D$_5$-NPh$_2$-D/H**, again suggesting the participation of [**1a**$^{-H}$**-Co**]$^{+}$.

Scheme 5. D/H exchange experiments informing the structure of a catalytically active cobalt species.

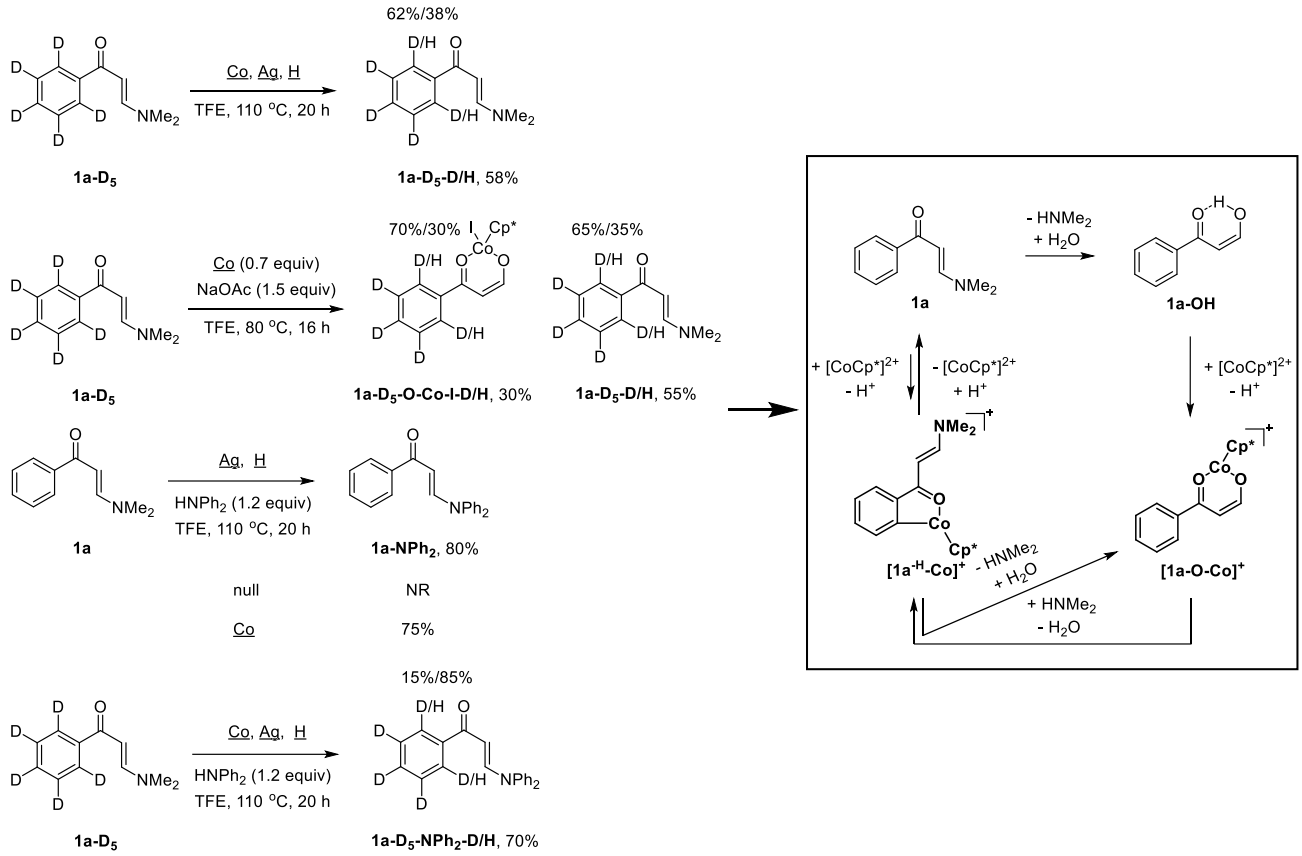

The dormant nature of [1a-O-Co]$^+$ and its relevance to productive catalysis ([1a^{-H}-Co]$^+$ delivered in the first round of catalysis by [1a-O-Co]$^+$/HNMe$_2$, slightly released from spontaneous hydrolysis of 1a) is verified by the catalytic competency of 1a-O-Co-I (Scheme 6). Further reinforcing the dormancy hypothesis is the ability of 1a-OH to participate in a catalytic reaction with 2a only through the assistance of a secondary amine (e.g., HNEt$_2$, HNPh$_2$). The role of secondary amine simply as a base is excluded by the failure of NEt$_3$, which is substitutionally inert toward 1a-OH, to promote the reaction. As an extra variant of catalysis, the engagement of HNEt$_2$ enables the reformulation of original reaction to the 1a-OH, 1a-O-Co-I format.

Scheme 6. Catalytic reactions highlighting the switching of cobalt species between the dormant and active states.

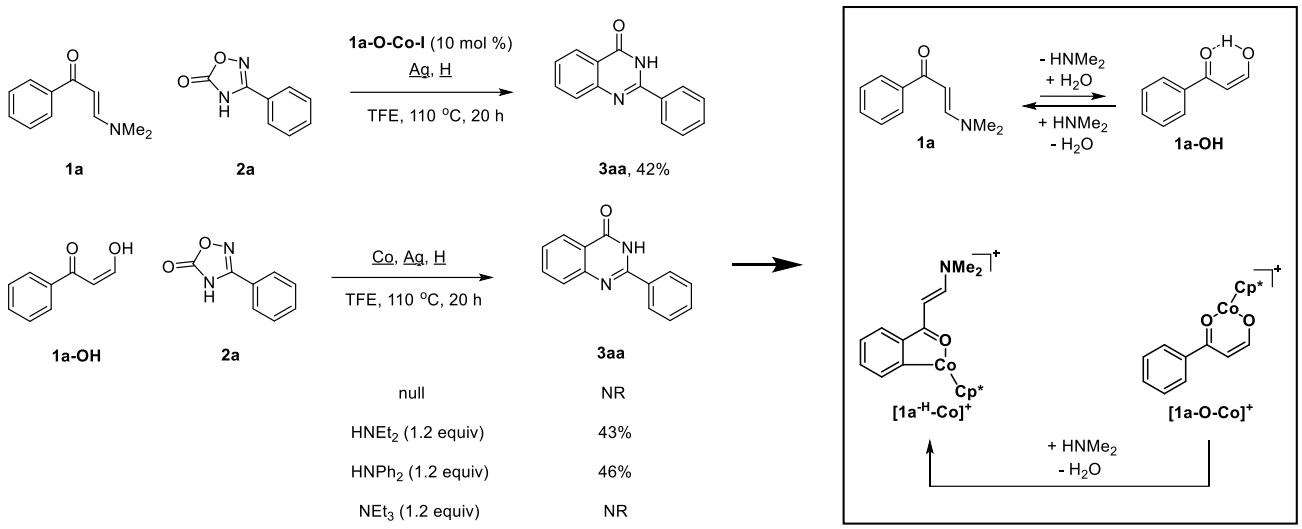

Collectively, the above mechanistic insight advocates proposal of the following dynamic covalent bonding exchange process (Scheme 7): equilibrium between **1a** (*E*-configuration) and **1a-OH** (*Z*-configuration, decomposed at 110 °C without coordination with cobalt) (reverse reaction favored, forward reaction at 110 °C, reverse reaction at lower than 110 °C), irreversible deprotonated coordination of **1a-OH** with cobalt complex to $[\mathbf{1a\text{-}O\text{-}Co}]^{+}$, isomerization of $[\mathbf{1a\text{-}O\text{-}Co}]^{+}$ to the aldehyde form $[\mathbf{1a\text{-}O\text{-}Co\text{-}iso}]^{2+}$ (the absence of internal hydrogen bonding might favor the aldehyde form upon protonation), substitution of $[\mathbf{1a\text{-}O\text{-}Co\text{-}iso}]^{2+}$ by $HNMe_2$ to a carbonyl- and vinyl-coordinated cobalt complex $[\mathbf{1a\text{-}Co}]^{2+}$, substitution of $[\mathbf{1a\text{-}Co}]^{2+}$ by H_2O to $[\mathbf{1a\text{-}O\text{-}Co}]^{+}$, equilibrium between $[\mathbf{1a\text{-}Co}]^{2+}$ and $[\mathbf{1a^{-H}\text{-}Co}]^{+}$, equilibrium between **1a**/cobalt complex and $[\mathbf{1a^{-H}\text{-}Co}]^{+}$ (reverse reaction favored).

Scheme 7. The proposed dynamic covalent bonding exchange process.

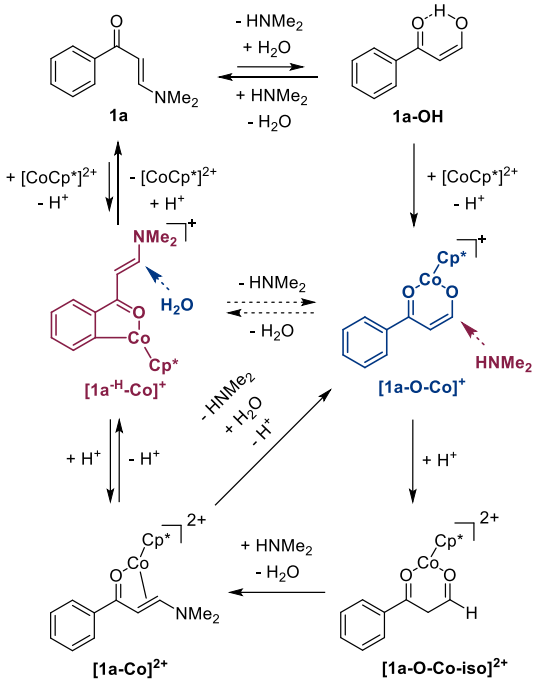

The C-N bond-forming process is interrogated by using ^{15}N (N4)-labeled **2a** (**2a-^{15}N**) as a replacement substrate for **2a** in the catalytic reaction with **1a** (Scheme 8). An exclusive ^{15}N labeling at N1 (**3aa-^{15}N**) without the scrambling of N atom, is observed. The C-C bond-cleavage process is investigated by the identification of by-products. However, no by-product can be initially spotted in the reaction mixture of **1a** and **2a**. Satisfactorily, employment of C_α-methylated **1a** (**1a-Me**) confirms acetone as one by-product; alteration of **1a** to **1a-NPh$_2$** reveals $HNPh_2$ as another by-product.

Scheme 8. ^{15}N isotope labeling and by-product analysis experiments revealing the bond formation and cleavage processes.

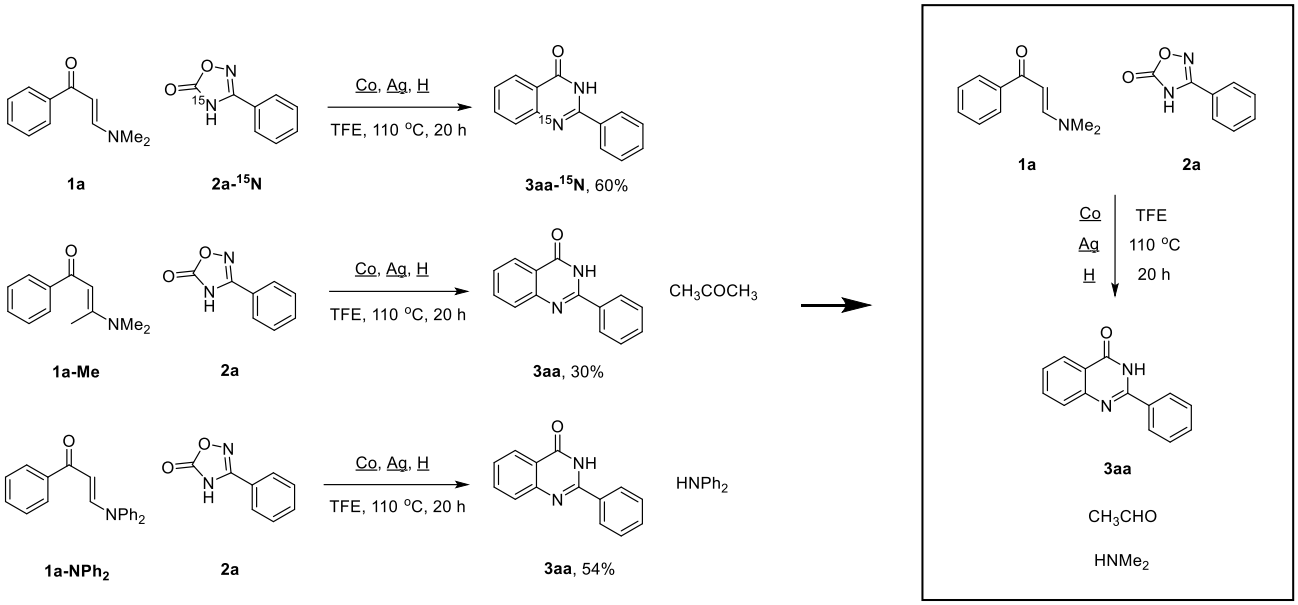

Taken together, the homeostatic catalysis system reported herein is proposed to operate through the following reaction course (Scheme 9): abstraction of iodide from $[CoCp*(CO)I_2]$ by $AgSbF_6$ to form $[CoCp*]^{2+}$ (**I**), **1a** hydrolysis generation of **1a-OH** and coordination with **I** to afford $[\mathbf{1a\text{-}O\text{-}Co}]^+$ (**II**), or alternatively, coordination of **I** with **1a** to furnish $[\mathbf{1a^{-H}\text{-}Co}]^+$ (**III**), dynamic covalent bonding equilibrium conversion between **II** and **III**, coordination of **III** with **2a** to produce **IV**, decarboxylative 1,1-migratory insertion to provide **V**, proto-demetalation to give **VI**, intramolecular N-C bond cyclization and C-C bond cleavage to deliver **3aa**.

Scheme 9. The proposed catalytic cycle.

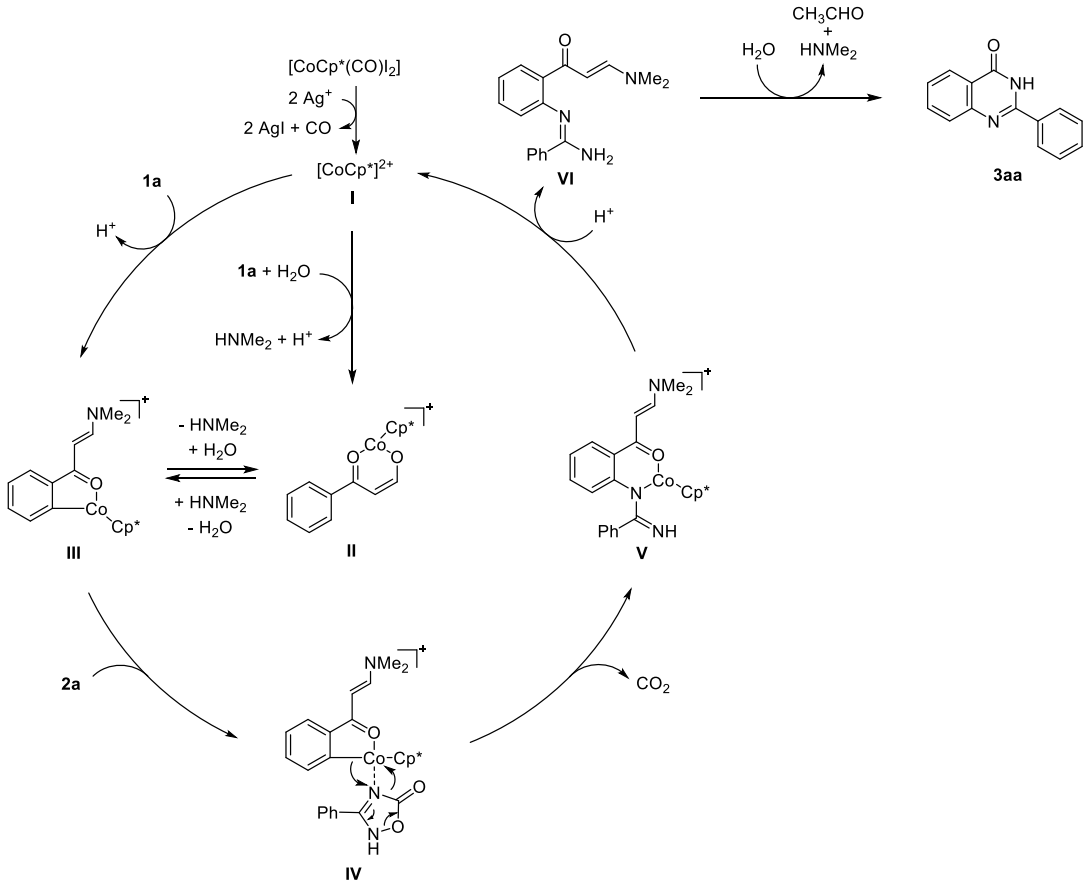

With the homeostatic catalysis products created herein, structural diversification and pharmaceutical agent manufacturing can be envisioned (Scheme 10). Indeed, ruthenium-catalyzed C-H bond activation in **3aa** enables its coupling with **4** to yield **5**.[37] Starting from **3aw**, schizocommunin (**6**), a fungal alkaloid that is cytotoxic against murine lymphoma cells by activating aryl hydrocarbon receptor gene battery, can be constructed by exploiting the nucleophilicity of methyl substituent.[38,39] This nucleophilicity of methyl group also allows the use of **3aw** in a three-step assembly of **7**, a potent promoter of p53 activity in rhabdomyosarcoma.[40,41] The methyl group can be rendered electrophilic by bromination for synthetic access to **8**, an inhibitor of tubulin assembly that shows anti-proliferative activity against HT29 cell line.[42] Another nucleophilic site on **3aw**, N3, can be harnessed for the synthesis of an anti-inflammatory and analgesic drug, diproqualone (**9**).[38,43]

Scheme 10. Structural diversification of quinazolinones into pharmaceutically active agents.

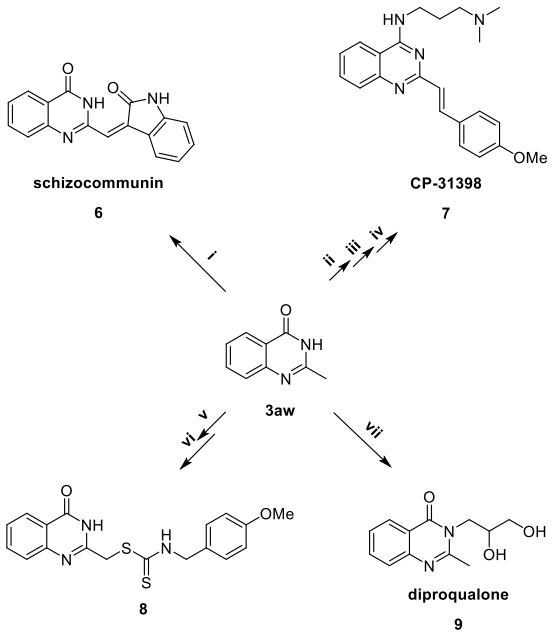

Conclusions

In conclusion, a cobalt homeostatic catalysis system has been developed for the coupling of enaminones and oxadiazolones to quinazolinones. The adventitious water-tolerant homeostasis has been demonstrated to operate through a dynamic covalent bonding-based mechanism: preferred C-N bond reactivity in enaminone toward water allows protected entry of cobalt species into a catalytically dormant state, and reverse exchange back by released $HNEt_2$ revives the dormant cobalt species to the catalytically active state. The conceptual proposal of such a homeostatic process can serve as an illustrative example of how the external hostile environment in catalysis can be reconciled in a productive way. With this efficient catalysis, a broad substrate scope is achieved and the quinazolinones produced thereof can serve as the starting point for further structural elaboration into diverse pharmaceutically active derivatives.

References

(1) Li, Z.; Wang, Z.; Chekshin, N.; Qian, S.; Qiao, J. X.; Cheng, P. T.; Yeung, K.-S.; Ewing, W. R.; Yu, J.-Q. A tautomeric ligand enables directed C-H hydroxylation with molecular oxygen. *Science* 2021, *372*, 1452-1457.

(2) Wang, F.; Jing, J.; Zhao, Y.; Zhu, X.; Zhang, X.; Zhao, L.; Hu, P.; Deng, W.; Li, X. Rhodium-catalyzed C-H activation-based construction of axially and centrally chiral indenes through two discrete insertions. *Angew. Chem. Int. Ed.* 2021, *60*, 16628-16633.

(3) Jacob, N.; Zaid, Y.; Oliveria, J. C. A.; Ackermann, L.; Wencel-Delord, J. Cobalt-catalyzed enantioselective C-H arylation of indoles. *J. Am. Chem. Soc.* 2022, *144*, 798-806.

(4) Hayler, J. D.; Leahy, D. K.; Simmons, E. M. A pharmaceutical industry perspective on sustainable metal catalysis. *Organometallics* 2019, *38*, 36-46.

(5) Hartwig, J. Organotransition Metal Chemistry: From Bonding to Catalysts; Universiy Science Books: New York, 2010.

(6) Hall, A. M. R.; Dong, P.; Codina, A.; Lowe, J. P.; Hintermair, U. Kinetics of asymmetric transfer hydrogenation, catalyst deactivation, and inhibition with Noyori complexes as revealed by real-time high-resolution flowNMR spectroscopy. *ACS Catal.* 2019, *9*, 2079-2090.

(7) Engel, J.; Smit, W.; Foscato, M.; Occhipinti, G.; Törnroos, K. W.; Jensen, V. R. Loss and reformation of ruthenium alkylidene: connecting olefin metathesis, catalyst deactivation, regeneration, and isomerization. *J. Am. Chem. Soc.* 2017, *139*, 16609-16619.

(8) Liu, D.; Daun, L.; Rodda, L. B.; Lu, E.; Xu, Y.; An, J.; Qiu, L.; Liu, F.; Looney, M. R.; Yang, Z.; Allen, C. D. C.; Li, Z.; Marson, A.; Cyster, J. G. CD97 promotes spleen dendritic cell homeostasis through the mechanosensing of red blood cells. *Science* 2022, *375*, eabi5965.

(9) Constantinides, M. G.; Belkaid, Y. Early-life imprinting of unconventional T cells and tissue homeostasis. *Science* 2021, *374*, eabf0095.

(10) Schwartz, W. R.; Ciuparu, D.; Pfefferle, L. D. Combustion of methane over palladium-based catalysts: catalytic deactivation and role of the support. *J. Phys. Chem. C* 2012, *116*, 8587-8593.

(11) Gholami, R.; Alyani, M.; Smith, K. J. Deactivation of Pd catalysts by water during low temperature methane oxidation relevant to natural gas vehicle converters. *Catalysts* 2015, *5*, 561-594.

(12) Sadeqzadeh, M.; Hong, J.; Fongarland, P.; Curulla-Ferré, D.; Luck, F.; Bousquet, J.; Schweich, D.; Khodakov, A. Y. Mechanistic modeling of cobalt based catalyst sintering in a fixed bed reactor under different conditions of Fischer-Tropsch synthesis. *Ind. Eng. Chem. Res.* 2012, *51*, 11955-11964.

(13) Leeuwen, P. W. N. M.; Chadwick, J. C. Homogeneous Catalysts; Wiley: Germany, 2011.

(14) Dinger, M. B.; Mol, J. C. Degradation of the first-generation Grubbs metathesis catalyst with primary alcohols, water, and oxygen. Formation and catalytic activity of ruthenium(Ⅱ) monocarbonyl species. *Organmetallics* 2003, *22*, 1089-1095.

(15) Kim, M.; Eum, M. S.; Jin, M. Y.; Jun, K. W.; Lee, C. W.; Kuen, K. A.; Kim, C. H.; Chin, C. S. Reactions of ruthenium benzylidenes with H_2O to give benzaldehyde and (aqua)ruthenium complex. *J. Organomet. Chem.* 2004, *689*, 3535-3540.

(16) Zhou, S.; Wang, J.; Wang, L.; Song, C.; Chen, K.; Zhu, J. Enaminones as synthons for a directed C-H functionalization: Rh^{III}-catalyzed synthesis of naphthalenes. *Angew. Chem. Int. Ed.* 2016, *55*, 9384-9388.

(17) Wang, Z.; Zhao, B.; Liu, Y.; Wan, J.-P. Recent advances in reactions using enaminone in water or aqueous medium. *Adv. Synth. Catal.* 2022, *364*, 1508-1521.

(18) Nagireddy, A.; Dattatri; Kotipalli, R.; Nanubolu, J. B.; Reddy, M. S. Rhodium-catalyzed regioselective double annulation of enaminones with propargyl alcohols: rapid access to arylnapthalene lignan derivatives. *J. Org. Chem.* 2022, *87*, 1240-1248.

(19) Fu, L.; Xu, W.; Pu, M.; Wu, Y.-D.; Liu, Y.; Wan, J.-P. Rh-catalyzed [4 + 2] annulation with a removable monodentate structure toward iminopyranes and pyranones by C-H annulation. *Org. Lett.* 2022, *24*, 3003-3008.

(20) Wang, F.; Jin, L.; Kong, L.; Li, X. Cobalt(Ⅲ)- and rhodium(Ⅲ)-catalyzed C-H amidation and synthesis of 4-quinolones: C-H activation assisted by weakly coordinating and functionalizable enaminone. *Org. Lett.* 2017, *19*, 1812-1815.

(21) Zhou, S.; Liu, D.-Y.; Wang, S.; Tian, J.-S.; Loh, T.-P. An efficient method for the synthesis of 2-pyridones via C-H bond functionalization. *Chem. Commun.* 2020, *56*, 15020-15023.

(22) Wu, W.; Fan, S.; Li, T.; Fang, L.; Chu, B.; Zhu, J. Cobalt-catalyzed, directed intermolecular C-H bond functionalization for multiheteroatom heterocycle synthesis: the case of benzotriazine. *Org. Lett.* 2021, *23*, 5652-5657.

(23) He, D.; Wang, M.; Zhao, S.; Shu, Y; Zeng, H.; Xiao, C.; Lu, C. Liu, Y. Pharmaceutical prospects of naturally occurring quinazolinone and its derivatives. *Fitoterapia* 2017, *119*, 136-149.

(24) Qian, Y.; Allegretta, G.; Janardhanan, J.; Peng, Z.; Mahasenan, K. V.; Lastochkin, E.; Gozun, M. M. N.; Tejera, Sara.; Schroeder, V. A.; Wolter, W. R.; Feltzer, R.; Mobashery, S.; Chang, M. Exploration of the structural space in 4(3*H*)-quinazolinone antibacterials. *J. Med. Chem*. 2020, *63*, 5287-5296.

(25) Zhang, J.; Liu, J.; Ma, Y.; Ren, D.; Cheng, P.; Zhao, J.; Zhang, F.; Yao, Y. One-pot synthesis and antifungal activity against plant pathogens of quinazolinone derivatives containing an amide moiety. *Bioorg. Med. Chem. Lett*. 2016, *26*, 2273-2277.

(26) Hemalatha, K.; Madhumitha, G. Inhibition of poly(adenosine diphosphate-ribose) polymerase using quinazolinone nucleus. *Appl. Microbiol. Biotechnol*. 2016, *100*, 7799-7814.

(27) Hirai, S.; Kikuchi, H.; Kim, H.-S.; Begum, K.; Wataya, Y.; Tasaka, H.; Miyazawa, Y.; Yamamoto, K.; Oshima, Y. Metabolites of febrifugine and its synthetic analogue by mouse liver S9 and their

antimalarial activity against plasmodium malaria parasite. *J. Med. Chem*. 2003, *46*, 4351-4359.

(28) Rudolph, J.; Esler, W. P.; O'Connor, S.; Coish, P. D. G.; Wickens, P. L.; Brands, M.; Bierer, D. E.; Bloomquist, B. T.; Bondar, G.; Chen, L.; Chuang, C.-Y.; Claus, T. H.; Fathi, Z.; Fu, W.; Khire, U. R.; Kristie, J. A.; Liu, X.-G.; Lowe, D. B.; McClure, A. C.; Michels, M.; Ortiz, A. A.; Ramsden, P. D.; Schoenleber, R. W.; Shelekhin, T. E.; Vakalopoulos, A.; Tang, W.; Wang, L.; Yi, L.; Gardell, S. J.; Livingston, J. N.; Sweet, L. J.; Bullock. W. H. Quinazolinone derivatives as orally available ghrelin receptor antagonists for the treatment of diabetes and obesity. *J. Med. Chem*. 2007, *50*, 5202-5216.

(29) Ugale, V. G.; Bari, S. B.; Khadse, S. C.; Reddy, P. N.; Bonde, C. G.; Chaudhari. P. J. Exploring quinazolinones as anticonvulsants by molecular fragmentation approach: structural optimization, synthesis and pharmacological evaluation studies. *ChemistrySelect* 2020, *5*, 2902-2912.

(30) Liu, K.; Li, D.; Zheng, W.; Shi, M.; Chen, Y.; Tang, M.; Yang, T.; Zhao, M.; Deng, D.; Zhang, C.; Liu, J.; Yuan, X.; Yang, Z.; Chen. L. Discovery, optimization, and evaluation of quinazolinone derivatives with novel linkers as orally efficacious phosphoinositide-3-kinase delta inhibitors for treatment of inflammatory diseases. *J. Med. Chem*. 2021, *64*, 8951-8970.

(31) Wang, J.; Mirzapoiazova, T.; Tan, Y.-H. C.; Pang, K. M.; Pozhitkov, A.; Wang, Y.; Wang, Y.; Mambetsariev, B.; Wang, E.; Nasser, M. W.; Batra, S. K.; Raz, D.; Reckamp, K.; Kulkarni, P.; Zheng, Y.; Salgia, R. Inhibiting crosstalk between MET signaling and mitochondrial dynamics and morphology: a novel therapeutic approach for lung cancer and mesothelioma. *Cancer Biol. Ther.* 2018, *19*, 1023-1032.

(32) Sakr, A.; Rezq, Samar.; Ibrahim, S. M.; Soliman, E.; Baraka, M. M.; Romero, D. G.; Kothayer, H. Design and synthesis of novel quinazolinones conjugated ibuprofen, indole acetamide, or thioacetohydrazide as selective COX-2 inhibitors: anti-inflammatory, analgesic and anticancer activities. *J. Enzym. Inhib. Med. Ch.* 2021, *36*, 1810-1828.

(33) Sun, J.; Tao, T.; Xu, D.; Gao, H.; Kong, Q.; Wang, X.; Liu, Y.; Zhao, J.; Wang, Y.; Pan, Y. Metal-free oxidative cyclization of 2-amino-benzamides, 2-aminobenzenesulfonamide or 2-(aminomethyl)anilines with primary alcohols for the synthesis of quinazolinones and their analogues. *Tetrahedron Lett.* **2018**, *59*, 2099-2102.

(34) Liu, X.; Fu, H.; Jiang, Y.; Zhao, Y. A simple and efficient approach to quinazolinones under mild copper-catalyzed conditions. *Angew. Chem. Int. Ed.* **2009**, *48*, 348-351.

(35) Wang, J.; Zha, S.; Chen, K.; Zhang, F.; Song, C.; Zhu, J. Quinazoline synthesis via Rh(III)-catalyzed intermolecular C-H functionalization of benzimidates with dioxazolones. *Org. Lett.* **2016**, *18*, 2062-2065.

(36) Xiong, H.; Xu, S.; Sun, S.; Cheng, J. Cp*Rh(III)-catalyzed annulation of *N*-methoxybenzamide with 1,4,2-bisoxazol-5-one toward 2-aryl quinazolin-4(3*H*)-one derivatives. *Org. Chem. Front.* **2018**, *5*, 2880-2884.

(37) Cai, P.; Zhang, E.; Wu, Y.; Fang, T.; Li, Q.; Yang, C.; Wang, J.; Shang, Y. Ru(II)/Ir(III)-catalyzed C-H bond activation/annulation of cyclic amides with 1,3-diketone-2-diazo compounds: Facile access to 8*H*-isoquinolino[1,2-*b*]quinazolin-8-ones and phthalazino[2,3-*a*]cinnoline-8,13-diones. *ACS Omega* **2018**, *3*, 14575-14584.

(38) Yang, J.; Hu, X.; Liu, Z.; Li, X.; Dong, Y.; Liu, G. Cp*Co^{III}-catalyzed formal [4 + 2] cycloaddition of benzamides to afford quinazolinone derivatives. *Chem. Commun.* **2019**, *55*, 13840-13843.

(39) Uehata, K.; Kimura, N.; Hasegawa, K.; Arai, S.; Nishida, M.; Hosoe, T.; Kawai, K.-I.; Nishida, A. Total synthesis of schizocommunin and revision of its structure. *J. Nat. Prod.* **2013**, *76*, 2034-2039.

(40) Mularski, J.; Malarz, K.; Pacholczyk, M.; Musiol, R. The p53 stabilizing agent CP-31398 and multi-kinase inhibitors. Designing, synthesizing and screening of styrylquinazoline series. *Eur. J. Med. Chem.* **2019**, *163*, 610-625.

(41) Xu, J.; Timares, L.; Heilpern, C.; Weng, Z.; Li, C.; Xu, H.; Pressey, J. G.; Elmets, C. A.; Kopelovich,

L.; Athar, M. Targeting wild-type and mutant p53 with small molecule CP-31398 blocks the growth of Rhabdomyosarcoma by inducing reactive oxygen species-dependent apoptosis. *Cancer Res.* 2010, *70*, 6566-6576.

(42) Ding, P.-P.; Gao, M.; Mao, B.-B.; Cao, S.-L.; Liu, C.-H.; Yang, C.-R.; Li, Z.-F.; Liao, J.; Zhao, H.; Li, Z.; Li, J.; Wang, H.; Xu, X. Synthesis and biological evaluation of quinazolin-4(3*H*)-one derivatives bearing dithiocarbamate side chain at C2-position as potential antitumor agents. *Eur. J. Med. Chem.* 2016, *108*, 364-373.

(43) Kumar, D.; Jadhavar, P. S.; Nautiyal, M.; Sharma, H.; Meena, P. K.; Adane, L.; Pancholia, S.; Chakraborti, A. K. Convenient synthesis of 2,3-disubstituted quinazolin-4(3*H*)-ones and 2-styryl-3-substituted quinazolin-4(3*H*)-ones: applications towards the synthesis of drugs. *RSC Adv.* 2015, *5*, 30819-30825.

Acknowledgments

We gratefully acknowledge support from the National Natural Science Foundation of China (52073141).